Bismutotantalite-stibiotantalite-stibiocolumbite assemblage from elbaite pegmatites at Molo near Momeik, northern Shan State, Myanmar

Novák Milan, Sejkora Jiří, Škoda Radek and Budina Václav

With 5 figures and 2 tables

Abstract: Bismutotantalite-stibiotantalite-stibiocolumbite (BSS) aggregates occur exclusively in pockets of the elbaite subtype pegmatites cutting serpentinized peridotite at Khetchel village, Molo quarter near Momeik Township, northeast of Mogok, Shan State, Myanmar (Burma). The pegmatites exhibit simple zoning with common pockets lined with K-feldspar, "mushroom-like" pink to red elbaite, beryl (aquamarine, morganite), petalite, phenakite, quartz, saccharoidal albite, adularia, hambergite and cookeite(?). The BSS aggregates consist of prismatic crystals of bismutotantalite-stibiotantalite (Bi/(Bi+Sb) = 0.47-0.51; Ta/(Ta+Nb) = 0.64-0.67; a = 5.6017(3), b = 11.7802(3), c = 4.9497(3) Å and V = 326.63(2) $Å^3$), up to about 5 mm in size, and their aggregates, up to 3 cm in diameter, forming ~ 95 vol.% of the overall BSS aggregate. Oval to irregular grains blebs of stibiotantalite (Bi/(Bi+Sb) = 0.04-0.08; Ta/(Ta+Nb) = 0.62-0.68), up to 100 μm in diameter, scarcely occur in bismutotantalite-stibiotantalite. Thin veinlets of stibiocolumbite (Bi/(Bi+Sb) = 0.01-0.05; Ta/(Ta+Nb) = 0.40-0.49) with brecciated textures, up to 30 μm thick, cut bismutotantalite-stibiotantalite and rarely also stibiotantalite blebs. Two distinct compositions were found in the stibiocolumbite veinlets, W-poor and rare W-rich (up to 19.34 wt.% WO_3). Late stibiocolumbite overgrowths (Bi/(Bi+Sb) = 0.01-0.03; Ta/(Ta+Nb) = 0.17-0.33) on crystals of bismutotantalite-stibiotantalite reach up to 20 μm in size. Bismutotantalite-stibiotantalite + stibiotantalite blebs → stibiocolumbite veinlets → stibiocolumbite overgrowths - is the succession of crystallization. All phases contain along with dominant Bi, Sb, Nb and Ta also low to moderate concentrations of some cations ($W^{6+} \leq 0.275$ apfu in stibiocolumbite veinlets, $Pb^{2+} \leq 0.052$ apfu, $Sn^{4+} \leq 0.010$ apfu, $As^{3+} \leq 0.032$ apfu; Ti ≤ 0.045 apfu and U ≤ 0.005 apfu, the latter two only in the stibiocolumbite overgrowths). High amounts of W in the stibiocolumbite veinlets change slightly ABO_4 stoichiometry from A/B ~1 to $\sum A$-site cations up to 1.216 apfu with $\sum A+B = 2.000$. The simple exchange vectors $Sb_1\ Bi_{-1}$ and $Nb_1\ Ta_{-1}$ are dominant in all phases examined, but the minor

substitution $Pb^{2+}{}_1W^{6+}{}_1$ $Sb^{3+}{}_{-1}Nb^{5+}{}_{-1}$ also was encountered in W-poor compositions. Fractionation in the BSS assemblage expressed by the Bi/(Bi+Sb) and Ta/(Ta+Nb) is asynchronous; the Bi/(Bi+Sb) value significantly drops down in the stibiotantalite blebs and it is very low in stibiocolumbite. Ta/(Ta+Nb) is constant in the bismutotantalite-stibiotantalite and stibiotantalite blebs, and then it decreases in the stibiocolumbite veinlets and particularly in the stibiocolumbite overgrowths.

Key words: bismutotantalite, stibiotantalite, stibiocolumbite, XRD powder diffraction, electron microprobe, substitutions, elbaite pegmatite, Molo, Myanmar

Introduction

Bismuth-dominant minerals of the stibiotantalite group (general formula ABO_4, where A = Sb,Bi and B = Nb,Ta) – bismutotantalite and bismutocolumbite - as well as stibiotantalite and stibiocolumbite with substantial amount of Bi are rare relative to the Bi-poor ones. They are known only from complex (Li-rich) pegmatites and a review of the bismutotantalite and bismutocolumbite localities was published by GALLISKI et al. (2001). Based on the descriptions available in literature, these pegmatites mostly belong to elbaite subtype (FOORD 1981, 1982, STERN et al. 1986, ZAGORSKYI & PERETYAZHKO 1992, PERETYAZHKO et al. 1992) and less commonly to lepidolite (BANNO et al. 2001), amblygonite (GALLISKI et al. 2001) and spodumene subtype (VOLOSHIN & PAKHOMOVSKYI 1988), respectively. Some descriptions of parental pegmatites are not sufficient to define the pegmatite subtype (e.g., v. KNORRING & MROSE 1962, v. KNORRING & FADIPE 1981). Bismutotantalite was also found as stream rounded pebbles (HURLBUT 1957).

Bismuth-dominant or Bi-rich members of the stibiotantalite group are compositionally quite heterogeneous and exhibit complicated textural relations (FOORD 1981, 1982, BANNO et al. 2001). We describe a new occurrence of texturally and compositionally complicated bismutotantalite-stibiotantalite-stibiocolumbite (BSS) aggregate from elbaite pegmatites at Khetchel village, Molo quarter near Momeik Township, northeast of Mogok, Shan State, Myanmar (Burma) in this paper. Substitution mechanisms and fractionation trends expressed by Bi/(Bi+Sb) and Ta/(Ta+Nb) values as well as behavior of minor cations (W, Pb, As, Sn, Ti) during evolution of the BSS assemblage were discussed.

Geological setting and description of parental pegmatites

The Mogok area, northern Shan State, Myanmar lies in the northern part of a narrow linear granitoid belt, about 1500 km in length and 50 km in width (KHIN ZAW 1998). This central granitoid belt comprises mesozonal granitoid plutons as well as highly evolved tin-tungsten granites, associated aplites and granitic pegmatites including the world-class tungsten-tin deposits such as Hermyingyi and Mawchi (KHIN ZAW 1998). Major episodes of granitoid emplacement occurred during late Cretaceous to early Eocene (see KHIN ZAW 1998). Based on the data given by KHIN ZAW (1998), the granitic pegmatites of this belt may be classified as beryl-columbite subtype (localities Gu Taungt, Payangazu, Taunggwa) and lepidolite subtype (the locality Sakangyi near Mogok) with large crystals of topaz. Their mineral assemblages suggest evident LCT signature (see ČERNÝ & ERCIT 2005).

Pegmatites from the Momeik region commonly form dikes and lenticular bodies, up to 2-5 m and exceptionally up to 10 m thick, which cut serpentinized peridotite body. The available information (U TIN HLAING & AUNG KHAING WION 2005) indicate that the pegmatites exhibit simple zoning with common pockets lined with crystals of K-feldspar, "mushroom-like" pink to red elbaite and Li-bearing olenite (ERTL et al. 2007), beryl (aquamarine, morganite), petalite, phenakite and hambergite. The other minerals found in the pegmatites include quartz, albite, schorl and muscovite. Elbaite as a dominat Li-carrier besides rare petalite, dominance of K-feldspar relative to albite particularly in pockets, almost entire absence of micas, and chemical composition of elbaite suggest that the pegmatites belong to the elbaite subtype of the complex type (NOVÁK & POVONDRA 1995, ČERNÝ & ERCIT 2005).

Analytical methods

Mineral phases of the BSS aggregate were analyzed using CAMECA SX 100 at the Joint Laboratory of Electron Microscopy and Microanalysis, Institute of Geological Sciences, Masaryk University, Brno and Czech Geological Survey, R. Škoda analyst. Element abundances of W, Nb, Ta, P, Ti, Zr, Hf, U, Th, Si, Y, Sc, Sb, Bi, As, Al, Pb, Mn, Mg, Fe, Ca and F were measured in wavelength dispersive mode. The following standards and X-ray lines were used. K_α lines: Ca - andradite, Fe - columbite, Mn - rhodonite, Ti - TiO; L_α lines: Nb - columbite, Sn - SnO_2, W - metallic W; L_β lines: Sb - metallic Sb; M_α lines: Pb - PbSe, Ta - $CrTa_2O_6$, and M_β lines: Bi -

metallic Bi, U - metallic U. The accelerating voltage and beam currents were 15 kV and 20 nA, respectively, with beam diameter 1 μm. Major elements were measured for 20 s at the peak and for 10 s for each background. The counting times for minor to trace elements were 40 s and 60 s, respectively, and half time on each background. When only one background and a calculated background slope were applied, the background counting time corresponded to the peak counting time. The raw data were reduced using appropriate PAP matrix corrections (POUCHOU & PICHOIR 1985). The normalization on 4 anions (oxygen) per formula unit was used.

The X-ray powder diffraction data were collected in Bragg-Brentano geometry on a PANalytical X´Pert PRO diffractometer equipped with X´Cellerator detector using CuK_α radiation (step-scanning 0.05°/500 s, curved graphite monochromator, 40 kV/30 mA). To minimize the complicated shape of the background due to classic glass sample holder, the studied samples were placed on the surface of a flat silicon wafer from alcoholic suspension. The positions and the intensities of the reflections were calculated using the Pearson VII profile shape function by ZDS program package (ONDRUŠ 1995). Unit cell-parameters were calculated using the program of BURNHAM (1962).

Results

Mineral assemblage of bismutotantalite-stibiotantalite-stibiocolumbite aggregate

The BSS aggregate occur exclusively in pockets lined with crystals of K-feldspar. Two types of K-feldspar were recognized. (i) Early, beige, subhedral crystals of K-feldspar I, up to 5 cm in size, are abundant. (ii) Late adularia (K-feldspar II) as white, euhedral crystals, up to 5 mm in diameter, is less common. Minor elbaite forms euhedral crystals and unusual, so called “mushroom” habit consisting of fibrous aggregates of rare black schorl to green elbaite in central parts and dominant pale pink to dark red elbaite in outer parts. Electron microprobe analyses of pink elbaite yielded high contents of Al (40.39-41.93 wt.% Al_2O_3), Si (36.27-37.79 wt.% SiO_2), low to moderate contents of Ca = 0.07-0.19 apfu (up to 1.08 wt.% CaO), Mn = 0.03-0.12 apfu (up to 0.88 wt.% MnO), and F = 0.31-0.33 apfu (up to 0.64 wt.% F) as well as low to moderate vacancy in the X-site (0.20-0.33 pfu). Lithium-bearing olenite with tetrahedrally coordinated B studied by ERTL et al. (2007) differs from the examined elbaite by low contents of Si (34.39 wt.% SiO_2), high Al (43.33 wt.% Al_2O_3), lower concentrations of Ca (0.49 wt.% CaO) and Mn (0.07 wt.% MnO). Fine-grained saccharoidal albite on K-feldspar I is rather rare as well as small grains of quartz and fine-grained aggregates of colorless chlorite (cookeite?). Several other minerals occur in pockets (U TIN HLAING

& AUNG KHAING WION 2005), but they have not been found associated with the BSS aggregate on the samples examined. High activity of B during pocket crystallization and perhaps during overall pegmatite evolution is evident from abundant elbaite and accessory hambergite. Low contents of F in elbaite (0.31-0.33 apfu) and in hambergite (< 0.02 apfu), derived from the refractive indices of hambergite measured by U TIN HLAING & AUNG KHAING WION (2005) using the method of NOVÁK et al. (1998), also suggest low activity of F. It is supported by the presence of petalite instead Li-micas and absence of pyrochlore group minerals as well.

Textural relations in the bismutotantalite-stibiotantalite-stibiocolumbite aggregate

The BSS aggregate, up to 3 cm in diameter, consists of subhedral to euhedral prismatic crystals of bismutotantalite-stibiotantalite, up to about 5 mm in size, ongrowing crystals of K-feldspar I in pockets. Rare individual crystals have brown to steel gray color with submetallic luster. On fresh surface, they are gray, dark yellow to brown with strong adamantine luster. Based on detailed textural and electron-microprobe study, four phases with distinctive paragenetic position, chemical composition and style of zoning were recognized. **Bismutotantalite-stibiotantalite** is volumetrically dominant forming ~ 95 vol.% of the BSS aggregate. Its subhedral to euhedral grains crystallized later than K-feldspar I. Their relationship to pink to red elbaite is not clear, bismutotantalite-stibiotantalite is older in most samples but some overlap with the crystallization of elbaite is very likely. In the BSE images, bismutotantalite-stibiotantalite is heterogeneous consisting of randomly distributed euhedral areas with faintly distinct shades of grey seen only using special offset (Fig. 1a). This zoned texture is similar, but less significant, relative to that found in bismutotantalite to Sb-rich bismutotantalite from Argentina (GALLISKI et al. 2001) and in Sb-rich bismutotantalite to Bi-rich stibiotantalite from Nagatare, Japan (BANNO et al. 2001). **Stibiotantalite blebs**, up to 100 μm in diameter, scarcely occur in bismutotantalite-stibiotantalite (Fig. 1b). They form oval to irregular grains with sharp contact. Simple zoning with two distinct zones is locally developed (Fig. 1b), but no textures resembling replacement of the host bismutotantalite-stibiotantalite were observed. **Stibiocolumbite veinlets** are more abundant relative to the stibiotantalite blebs. Thin irregular veinlets, up to 30 μm thick, cut bismutotantalite-stibiotantalite and rarely also stibiotantalite blebs. They locally exhibit brecciated textures and asymmetrical zoning in the BSE image (Fig 1b). These textures generally suggest that early bismutotantalite-stibiotantalite was replaced by Nb-rich member of the stibiotantalite group – stibiocolumbite; however, the textures showing evident replacement features on the contact between host bismutotantalite-stibiotantalite and/or stibiotantalite blebs and veinlets are not convincing (Fig. 1b).

Two distinct compositions were found in stibiocolumbite veining, W-poor and rare W-rich one, but their recognition in a routine BSE image is uneasy. Late **stibiocolumbite overgrowths** on crystals of bismutotantalite-stibiotantalite reach up to 20 μm in size. They are very rare relative to the other Bi,Sb,Ta,Nb-phases given above. The individual overgrowths exhibit irregular zoning in the BSE image (Fig. 1b). The succession of crystallization in the BSS aggregate is: bismutotantalite-stibiotantalite + stibiotantalite blebs → stibiocolumbite veinlets → stibiocolumbite overgrowths. Disregarding intensive searching, no pyrochlore group minerals were detected in this assemblage.

Structural characterization of bismutotantalite-stibiotantalite-stibiocolumbite aggregate

XRD powder diffraction data were obtained for the dominant bismutotantalite-stibiotantalite of the complex BSS aggregate; the volume of the other associated phases is negligible to be recognizable using a routine X-ray powder diffraction and, moreover, all potential phases have very similar powder diffraction patterns. The data fit very well with those published for bismutotantalite and stibiotantalite (GALLISKI et al. 2001, ZUBKOVA et al. 2002) with variable Bi/(Bi+Sb) and Ta/(Ta+Nb) ratios (Table 1). The obtained data were indexed using the data calculated from the Lazy Pulverix program (YVON et al. 1977) by analogy with natural and synthetic bismutotantalite and stibiotantalite (PONOMAREV et al. 1981, KAZANTSEV et al. 2002). The space groups *Pnna* (usually Bi > Sb) and $Pna2_1$ (usually Bi < Sb) are characteristic for the minerals of the stibiotantalite group (GALLISKI et al. 2001; ZUBKOVA et al. 2002). The participation of the centrosymmetric *Pnna* or acentric $Pna2_1$ space groups in the $(Bi,Sb)(Nb,Ta)O_4$ phases is attributed to the different stereochemical activities of the lone pairs of electrons associated with Bi^{3+} and Sb^{3+} ions (GALY et al. 1975, ZUBKOVA et al. 2002). The theoretical data were calculated for both space groups using the identical unit-cell parameters and sites occupancies obtained from the chemical compositions. They were compared with the experimental patterns. Considering better results of diffraction intensities in comparison both space groups, the space group *Pnna* seems more probable (cf. GALLISKI et al. 2001), but recognition of the space group solely using the X-ray powder data is not possible.

Chemical composition of bismutotantalite-stibiotantalite-stibiocolumbite aggregate

Bismutotantalite-stibiotantalite exhibits low variation in Bi/(Bi+Sb) = 0.47-0.51 (Fig. 2). Minor cations in the *A*-site (Bi^{3+}, Sb^{3+} >> Pb^{2+}, As^{3+}, Sn^{4+}) include Pb (0.021-0.045 apfu; ≤ 2.64 wt.% PbO), and traces of Sn (≤ 0.010 apfu; ≤ 0.40 wt.% SnO_2) and As (≤ 0.006 apfu; ≤ 0.15 wt.%

As_2O_3). The very narrow span of the Ta/(Ta+Nb) = 0.64-0.67 and low concentrations of W (0.018-0.056 apfu; ≤ 3.38 wt.% WO_3) are typical in the *B*-site (Nb^{5+}, Ta^{5+} >> W^{6+}) (Table 2, Fig. 2). **Stibiotantalite blebs** show low Bi/(Bi+Sb) = 0.04-0.08, but the other chemical characteristics are similar to bismutotantalite-stibiotantalite: Ta/(Ta+Nb) = 0.62-0.68, W (0.035-0.049 apfu; ≤ 3.20 wt.% WO_3). Slightly higher Pb (0.043-0.052 apfu; ≤ 3.31 wt.% PbO) and As (≤ 0.025 apfu; ≤ 0.71 wt.% As_2O_3), and traces of Sn (≤ 0.005 apfu; ≤ 0.23 wt.% SnO_2) also were found (Table 2). Weak zoning in the BSE image (Fig. 1b) in bismutotantalite-stibiotantalite and stibiotantalite blebs is very likely controlled by variation in Bi/(Bi+Sb) and Ta/(Ta+Nb). **Stibiocolumbite veining** has more heterogeneous composition. Tungsten-poor compositions exhibits low and almost constant Bi/(Bi+Sb) = 0.04-0.05, low variation in Ta/(Ta+Nb) = 0.43-0.49 and low W (0.045-0.053 apfu; ≤ 3.76 wt.% WO_3). Concentrations of minor cations Pb (0.042-0.046 apfu; ≤ 3.11 wt.% PbO), As (≤ 0.024 apfu; ≤ 0.72 wt.% As_2O_3) and traces of Sn (≤ 0.007 apfu; ≤ 0.34 wt.% SnO_2) are comparable to the above phases (Table 2). Tungsten-rich compositions have very low Bi/(Bi+Sb) = 0.01 and moderate Ta/(Ta+Nb) = 0.40-0.45, but high contents of W (0.251-0.275 apfu; 17.81-19.34 wt. % WO_3). The other chemical characteristics (contents of As and Sn) are comparable to the W-poor compositions except very low Pb (≤ 0.007 apfu; ≤ 0.50 wt.% PbO). **Stibiocolumbite overgrowths** show very low Bi/(Bi+Sb) = 0.01-0.03 and low to moderate Ta/(Ta+Nb) = 0.17-0.33, low but variable W (0.031-0.088 apfu; ≤ 6.86 wt.% WO_3) and Pb (0.024-0.045 apfu; ≤ 3.44 wt.% PbO). Low contents of As (≤ 0.023 apfu; (0.77 wt.% As_2O_3) and traces of Sn (≤ 0.009 apfu; ≤ 0.46 wt.% SnO_2) also were found. Presence of minor to trace amounts of Ti (0.022-0.045 apfu; ≤ 1.20 wt.% TiO_2) and U (≤ 0.005 apfu; ≤ 0.44 wt.% UO_2) is typical only for the stibiocolumbite overgrowths.

From early to late phases general decrease of Bi/(Bi+Sb) and Ta/(Ta+Nb) are evident (Fig. 3). Behavior of W is more erratic and opposite to behavior of Nb (Fig. 3). Low contents of W are typical for early bismutotantalite-stibiotantalite and stibiotantalite blebs but variable and locally high in stibiocolumbite veinlets, and moderate to low in late stibiocolumbite overgrowths (Fig. 3). Concentrations of minor to trace cations (Pb, As, Sn) show low variations in the individual phases recognized. The chemical analyses yielded *A*/*B* ratio close to 1 (Table 2). The compositions usually show slightly higher sum of cations, up to 2.030 apfu, slight dominance of *A*-site cations over *B*-site ones, which is evidently higher in the W-rich compositions with ∑*A*-site cations up to 1.216 apfu.

Discussion

Chemical composition and substitutions

Both early phases bismutotantalite-stibiotantalite and stibiotantalite blebs contain along with dominant Bi, Sb, Nb and Ta also concentrations of minor cations (Pb^{2+}, As^{3+}, Sn^{4+} and W^{6+}). Stibiocolumbite veining exhibits variable and locally high contents of W, up to 0.275 apfu (Fig. 3), which are much higher relative to the other W-enriched minerals of the stibiotantalite group (e.g., FOORD 1982). However, W was determined only in some published analyses (e.g., FOORD 1981, 1982, GALLISKI et al. 2001, NOVÁK & ČERNÝ 1998, ČERNÝ et al. 2004, NOVÁK et al. 2004); hence, minor contents of W in the minerals of stibiotantalite group are very likely more common.

The chemical compositions (Table 2) suggest dominant homovalent substitutions expressed as simple exchange vectors

$$Sb_1\ Bi_{-1} \text{ and } Nb_1\ Ta_{-1} \qquad [1,2]$$

in all phases examined; however, their participation is distinct. The $Sb_1\ Bi_{-1}$ substitution is moderate in bismutotantalite-stibiotantalite but significant in stibiotantalite blebs and other phases. The $Nb_1\ Ta_{-1}$ substitution is moderate in bismutotantalite-stibiotantalite and stibiotantalite blebs but high in stibiocolumbite veining and chiefly in stibiocolumbite overgrowths (Fig. 1b). Incorporation of W into stibiocolumbite structure requires a heterovalent substitution. Positive correlation W *versus* Pb close to 1 (Fig. 4a) suggests the substitution

$$Pb^{2+}{}_1W^{6+}{}_1\ Sb^{3+}{}_{-1}Nb^{5+}{}_{-1} \qquad [3]$$

for the majority of compositions with low concentrations of W. Stibiocolumbite overgrowths exhibit in most plots distinct trends (Fig. 4, 5). Positive correlations Pb *versus* W (Fig. 4a), W *versus* Ti+Sn (Fig. 4b) and Pb *versus* Ti+Sn (Fig. 4c) and negative correlation Ti+Sn versus Nb+Ta (Fig. 4d) indicate combination of several substitutions such as

$$Pb^{2+}{}_1(Sn^{4+},Ti^{4+})_1W^{6+}{}_2\ (Sb^{3+},Bi^{3+})_{-1}(Nb^{5+},Ta^{5+})_{-3} \qquad [4]$$

and probably also

$$Pb^{2+}{}_1\ (Sn^{4+},Ti^{4+})_1\ (Sb^{3+},Bi^{3+})_{-2} \qquad [5]$$

(see also Fig. 5); however, low number of analyses does not enable reliable elucidation of the substitution mechanism. High amounts of W in the stibiocolumbite veining change ABO_4 stoichiometry to surplus of the *A*-site cations. Very small W-rich areas in stibiocolumbite veining, about 20 μm in diameter, do not allow more detailed study.

Fractionation trends

Fractionation in the BSS assemblage expressed by the Bi/(Bi+Sb) and Ta/(Ta+Nb) values is evident. Both values decrease during evolution, but this decreasing is asynchronous (Fig. 2, 3). The

Bi/(Bi+Sb) value drops down very quickly even within the stibiotantalite blebs and it is very low in the stibiocolumbite veining. Ta/(Ta+Nb) remains almost the same in the stibiotantalite blebs (Fig. 2, 3), which originated likely simultaneously with the host bismutotantalite-stibiotantalite. Ta/(Ta+Nb) decreases in the stibiocolumbite veining and particularly in the stibiocolumbite overgrowths. An appearance of Ti in the latest stages (stibiocolumbite overgrowths) indicates opening (see also increased amount of U) of the system or crystal-structural constraints.

Comparison of the bismutotantalite-stibiotantalite-stibiocolumbite aggregate with other localities

This comparison is complicated because a large set of detected elements including W, Pb, As and detailed description of zonality in bismutotantalite and other Bi-rich minerals of stibiotantalite group from BSE images is only exceptionally given in literature (FOORD 1981, 1982, BANNO et al. 2001, GALLISKI et al. 2001). The chemical composition of primary bismutotantalite-stibiotantalite and presence of late veining found at Momeik is similar to those of Nagatare, Japan (BANNO et al. 2001). Both localities exhibit decreasing of Bi/(Bi+Sb) and Ta/(Ta+Nb) in veining relative to a primary phase, but this difference is much higher at Momeik (Fig. 3). Heterogeneous bismutotantalite and bismutotantalite-stibiotantalite consisting of euhedral portions with slightly different composition were found in Nagatare, Japan (BANNO et al. 2001) as well as in Argentina (GALLISKI et al. 2001). These localities also show absence of late replacement by pyrochlore group minerals found at some other localities (e.g., v. KNORRING & FADIPE 1981, ČERNÝ & ERCIT 1985, 1989, VOLOSHIN et al. 1983). Poor descriptions of chemical composition, zonality and mineral assemblages at some well-known localities of bismutotantalite in Brazil and Africa (e.g., HURLBUT 1957, v. KNORRING & FADIPE 1981), however, do not enable any detailed comparison.

Conclusions

The BSS aggregate from Momeik, Mogok area, Myanmar exhibits complicated chemical composition and textural relations. It generally shows compositional evolution from early phases with high to moderate Bi/(Bi+Sb) and Ta/(Ta+Nb) to late phases with low Bi/(Bi+Sb) and low to moderate Ta/(Ta+Nb) (cf. BANNO et al. 2001), but this decrease is not simultaneous (Fig. 3). Textural relations of the stibiocolumbite veining and stibiocolumbite overgrowths suggest that they are later; nevertheless, textural features of replacement of early phases are not well developed. Also

no replacement of this assemblage by pyrochlore group minerals has been found. Besides dominant homovalent substitutions Sb_1 Bi_{-1} and Nb_1 Ta_{-1} described elsewhere (e.g., BANNO et al. 2001, ČERNÝ et al. 2004), W-poor phases of the BSS assemblage show heterovalent substitution $Pb^{2+}{}_1W^{6+}{}_1$ $Sb^{3+}{}_{-1}Nb^{5+}{}_{-1}$ unknown to date in the stibiotantalite group minerals (ČERNÝ et al. 2004). This suggests that it is necessary to analyze also potential minor cations such as Pb, Sn, As, Sc, W, and Ti in this mineral group to reveal actual substitution mechanisms.

Acknowledgements

The authors are very grateful to an anonymous reviewer and to A. Beran for the editorial improvements. The authors thank J. Plášil (Faculty of Science, Charles University, Prague) for technical assistance. The work was supported by Granting Agency of the Czech Republic, Grant No. 205/07/1159 to MN, and by the grant MK00002327201 of Ministry of Culture of the Czech Republic to JS.

References

BANNO, Y., BUNNO, M., HARUNA, M. & OBA, M. (2001): Stibiotantalite-group minerals in a lithium pegmatite from Nagatare, Fukuoka Prefecture, Japan. - Journ. Mineral. Petrol. Sci., **96**: 205-209.

BURNHAM, CH. W. (1962): Lattice constant refinement. - Carnegie Inst. Washington Year Book, **61:** 132-135.

ČERNÝ, P., CHAPMAN, R., FERREIRA, K. & SMEDS, S.-A. (2004): Geochemistry of oxide minerals of Nb, Ta, Sn and Sb in the Varuträsk granitic pegmatite, Sweden. - Amer. Mineral., **89**: 505-518.

ČERNÝ, P. & ERCIT, S.T. (1985): Some recent advances in the mineralogy and geochemistry of Nb and Ta in rare-element granitic pegmatites. - Bull. Minéral., **108**: 499-532.

ČERNÝ, P. & ERCIT, S.T. (1989): Mineralogy of Niobium and Tantalum: Crystal Chemical Relationships, Paragenetic Aspects and Their Economic Implications. - In: P. MÖLLER, P. ČERNÝ & F. SAUPE (Eds.): Lanthanides, Tantalum and Niobium, Springer Verlag Berlin Heidelberg, 27-79.

ČERNÝ, P. & ERCIT, T.S. (2005): The classification of granitic pegmatites revisited. - Canad. Mineral., **43**: 2005-2026.

ERTL, A., HUGHES, J.M., PROWATKE, S., LUDWIG, T., BRADSTÄTTER, F., KORNER, W. & DYAR, M.D. (2007): Tetrahedrally coordinated boron in Li-bearing olenite from "mushroom" tourmaline from Momeik, Myanmar. - Canad. Mineral., **45**: 891-899.

FOORD, E.E. (1981): Bismuthian stibiocolumbite-tantalite and other minerals from the Little Three Mine, Ramona, California. - Amer. Mineral., **67**: 181-182.

FOORD, E.E. (1982): Minerals of tin, titanium, niobium and tantalum in granitic pegmatites. - In: ČERNÝ, P. (Ed.): MAC Short Course Handbook 8, 187-238.

GALY, J., MEUNIER, G., ANDERSSON, A. & ÅSTRÖM, A. (1975): Stéréochimie des éléments comportans des paires non liées: Ge(II), As(III), Se(IV), Br(V), Sn(II), Sb(III), Te(IV), I(V), Xe(VI), Tl(I), Pb(II) et Bi(III) (oxydes, fluorures et oxyfluorures). - J. Solid State Chem., **13**: 142-159.

GALLISKI, M.A., MÁRQUEZ-ZAVALÍA, M.F., COOPER, M.A., ČERNÝ, P. & HAWTHORNE, F.C. (2001): Bismutotantalite from northwestern Argentina: description and crystal structure. - Canad. Mineral., **39**: 103-110.

HURLBUT, C.S. jr. (1957): Bismutotantalite from Brazil. - Amer. Mineral., **42**: 178-183.

KAZANTSEV, S.S., PUSHCHAROVSKYI, D.YU., MAXIMOV, B.A., MOLCHANOV, V.N., WERNER, S., SCHNEIDER, J. & SAPOZHNIKOV, A.N. (2002): Phase transitions in solid solution series bismutocolumbite - stibiocolumbite (Bi,Sb)($Nb_{0.79}Ta_{0.21}$)O_4. - Zeit. Krist., **217:** 542-549.

V. KNORRING, O. & FADIPE, A. (1981): On the mineralogy and geochemistry of niobium and tantalum in some granite pegmatites and alkali granites of Africa. - Bull. Minéral., **104**: 496-507.

V. KNORRING, O. & MROSE, M.E. (1962): Westgrenite and waylandite; two new bismuth minerals from Uganda. - Prog. Abstr. 1962 Ann. Meeting GSA-MSA, 156A.

NOVÁK, M., BURNS, P.C. & MORGAN, G.B.VI (1998): Fluorine variation in hambergite from granitic pegmatites. - Canad. Miner., **36**: 441-446.

NOVÁK, M. & ČERNÝ, P. (1998): Niobium-tantalum oxide minerals from complex pegmatites in the Moldanubicum, Czech Republic; Primary *versus* secondary compositional trends. - Canad. Mineral., **36**: 659-672.

NOVÁK, M., ČERNÝ, P., CEMPÍREK, J., ŠREIN, V. & FILIP, J. (2004): Ferrotapiolite as a pseudomorph of stibiotantalite from the Laštovičky lepidolite pegmatite, Czech Republic; an example of hydrothermal alteration at constant Ta/(Ta+Nb). - Canad. Miner., **42**: 1117-1128.

NOVÁK, M. & POVONDRA, P. (1995): Elbaite pegmatites in the Moldanubicum: a new subtype of the rare-element class. - Mineral. Petrol., **55**: 159-176.

ONDRUŠ, P. (1995): ZDS - software for analysis of X-ray powder diffraction patterns. Version 6.01. User´s guide. - 208 pp.

PERETYAZHKO, I.S., ZAGORSKYI, V.E., SAPOZHNIKOV, A.N., BOBROV, YU. D. & RAKCHEEV, A.D. (1992): Bismutocolumbite $Bi(Nb,Ta)_4$ – a new mineral from the miarol pegmatites. - Zap. Vsesoz. Mineral. Obshch., **121**: 130-134. (In Russian).

PONOMAREV, V.I., FILIPENKO, O.S., ATOVMYAN, L.O., RANNEV, N.V., IVANOV, S. & VENEVTSEV, YU.N. (1981): Structure and lattice dynamics of $SbNbO_4$ crystals at 300-1000 K. - Kristallografiya, **26**: 341-348. (In Russian).

POUCHOU, J.L. & PICHOIR, F. **(**1985): "PAP"(φ–ρ–Z) procedure for improved quantitative microanalysis. - In: ARMSTRONG, J.T. (Ed.): Microbeam Analysis, San Francisco Press, 104-106.

STERN, L.A., BROWN, G.E., JR., BIRD, D.K., JAHNS, R.H., FOORD, E.E., SHIOGLEY, J.E. & SPAULDING, L.B., JR. (1986): Mineralogy and geochemical evolution of the Little Three pegmatite-aplite layered intrusive, Ramona, California. - Amer. Mineral., **71**: 406-427.

U TIN TIN HLAING & AUNG KHAING WION (2005): Rubellite and other gemstones from Momeik township, northern Shan State, Myanmar. - Austral. Gemmol., **22**: 215-218.

VOLOSHIN, A.V., PAKHOMOVSKYI, YA.A., STEPANOV, V.I. & TYUSHEVA, F.N. (1983): Natrobistantite $(Na,Cs)Bi(Ta,Nb,Sb)_4O_{12}$ – a new mineral from granitic pegmatites. - Mineral. Zh., **5**: 82-86. (In Russian).

VOLOSHIN, A.V., & PAKHOMOVSKYI, YA.A. (1988): Mineralogy of tantalum and niobium in rare-elements pegmatites. - Nauka, Leningrad, Russia. (In Russian).

YVON, K., JEITSCHKO, W. & PARTHÉ, E. (1977): Lazy Pulverix, a computer program for calculation X-ray and neutron diffraction powder patterns. - J. Appl. Cryst., **10**: 73-74.

ZAGORSKYI, V.E. & PERETYAZHKO, I.C. (1992): Pegmatites with gemstones of Central Transbaikalia. - Nauka, Novosibirsk. 221 p. (In Russian).

ZAW KHIN (1998): Geological evolution of selected granitic pegmatites in Myanmar (Burma): constraints from regional setting, lithology, and fluid inclusion studies. - Internat. Geol. Review, **40**: 647-662.

ZUBKOVA, N.V., PUSCHAROVSKYI, D.YU., GIESTER, G., SMOLIN, A.S., TILLMANNS, E., BRANDSTÄTTER, F., HAMMER, V., PERETYAZHKO, I.S., SAPOZHNIKOV, A.N. & KASHAEV, A.A. (2002): Bismutocolumbite, $Bi(Nb_{0.79}Ta_{0.21})O_4$, stibiocolumbite, $Sb(Nb_{0.67}Ta_{0.33})O_4$, and their structural relation to the other ABO_4 minerals with stibiotantalite ($SbTaO_4$) structure. - N. Jb. Miner. Mh., **4**: 145-159.

Received:
Responsible editor:

Author's addresses:

NOVÁK MILAN, ŠKODA RADEK, Department of Geological Sciences, Masaryk University, Kotlářská 2, 611 37 Brno, Czech Republic. E-mail: mnovak@sci.muni.cz, rskoda@sci.muni.cz

SEJKORA JIŘÍ, Department of Mineralogy and Petrology, National Museum, Václavské nám. 68, 115 79 Praha 1, Czech Republic. E-mail: jiri.sejkora@nm.cz

BUDINA VÁCLAV, KARP, Politických vězňů 82, 261 02 Příbram, Czech Republic

Figure captions:

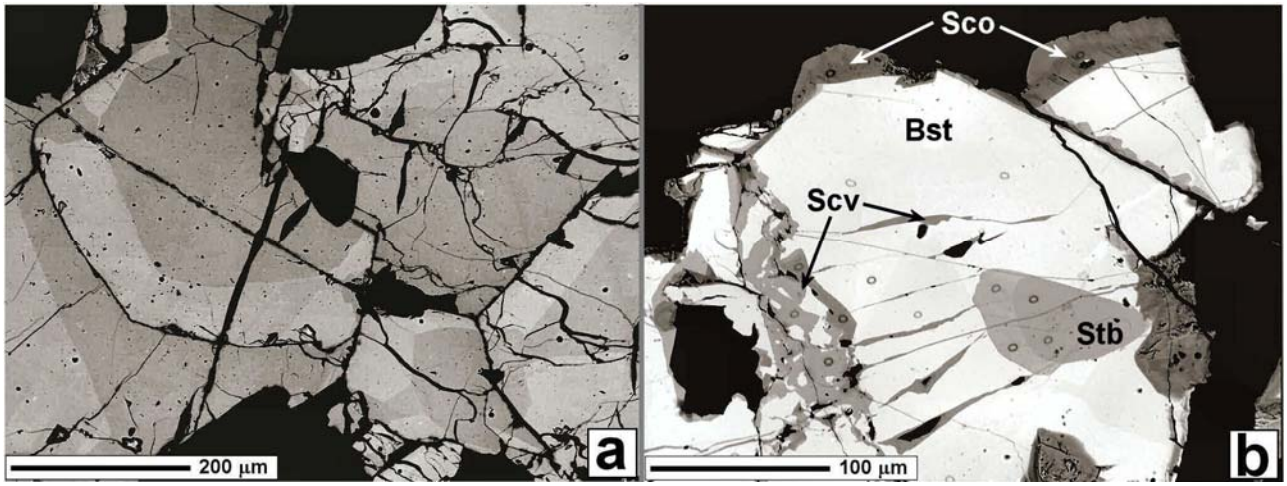

Fig. 1. BSE image of the bismutotantalite-stibiotantalite-stibiocolumbite assemblage; a) heterogeneous primary bismutotantalite-stibiotantalite; b) bismutotantalite-stibiotantalite (Bst) with stibiotantalite bleb (Stb), stibiocolumbite veinlets (Scv) and stibiocolumbite overgrowths (Sco), note zoned internal structure of bleb, veinlets and overgrowths and brecciated character of veinlets. Circular spots in b) are burn marks in the carbon coating.

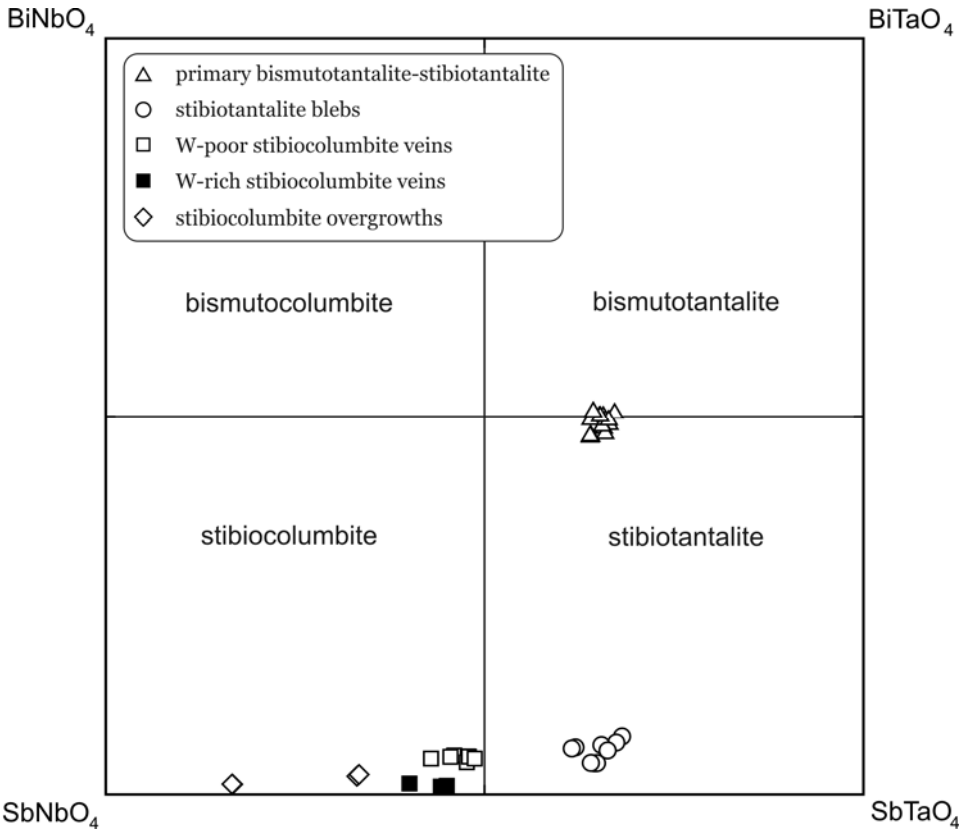

Fig. 2. Composition of bismutotantalite-stibiotantalite-stibiocolumbite assemblage in the stibiotantalite quadrilateral, Bi/(Bi+Sb) *versus* Ta/(Ta+Nb).

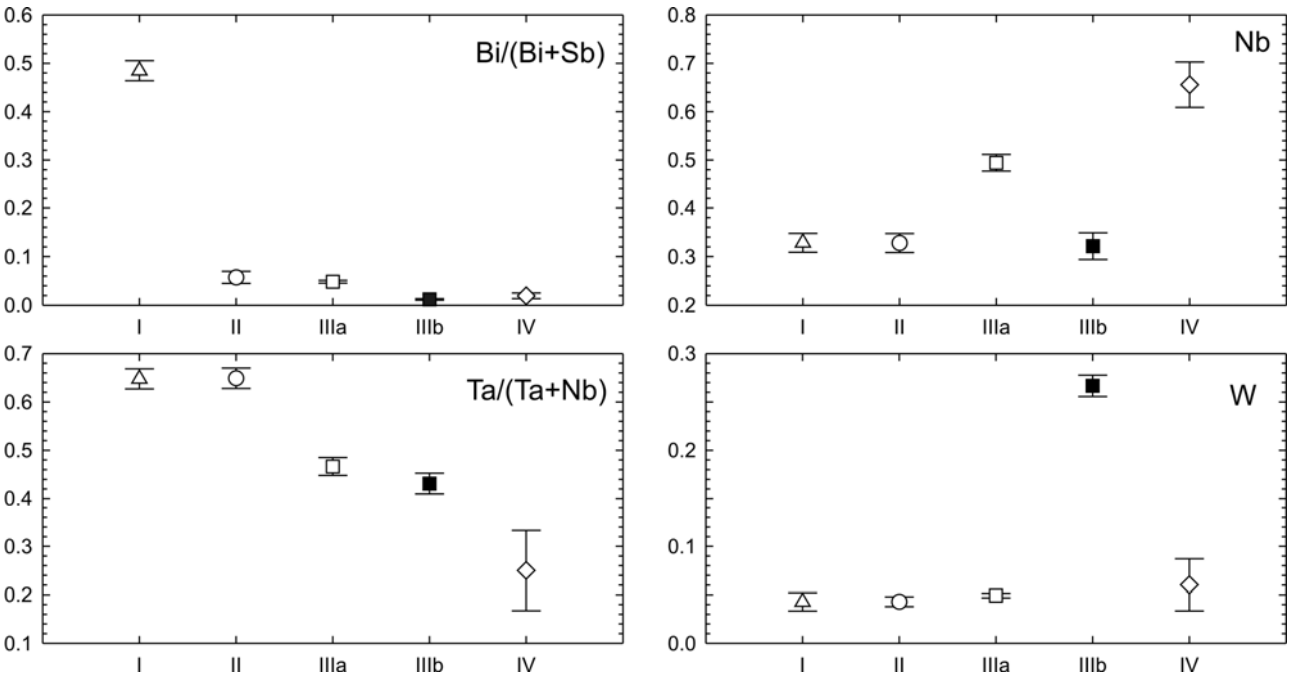

Fig. 3. Diagrams showing compositional evolution in the individual phases of the bismutotantalite-stibiotantalite-stibiocolumbite assemblage in the terms Bi/(Bi+Sb), Ta/(Ta+Nb), Nb and W. I - bismutotantalite-stibiotantalite, II - stibiotantalite blebs; IIIa – stibiocolumbite veinlets, W-poor compositions; IIIb - stibiocolumbite veinlets, W-rich compositions; IV - stibiocolumbite overgrowths; otherwise the same symbols as in Fig. 2.

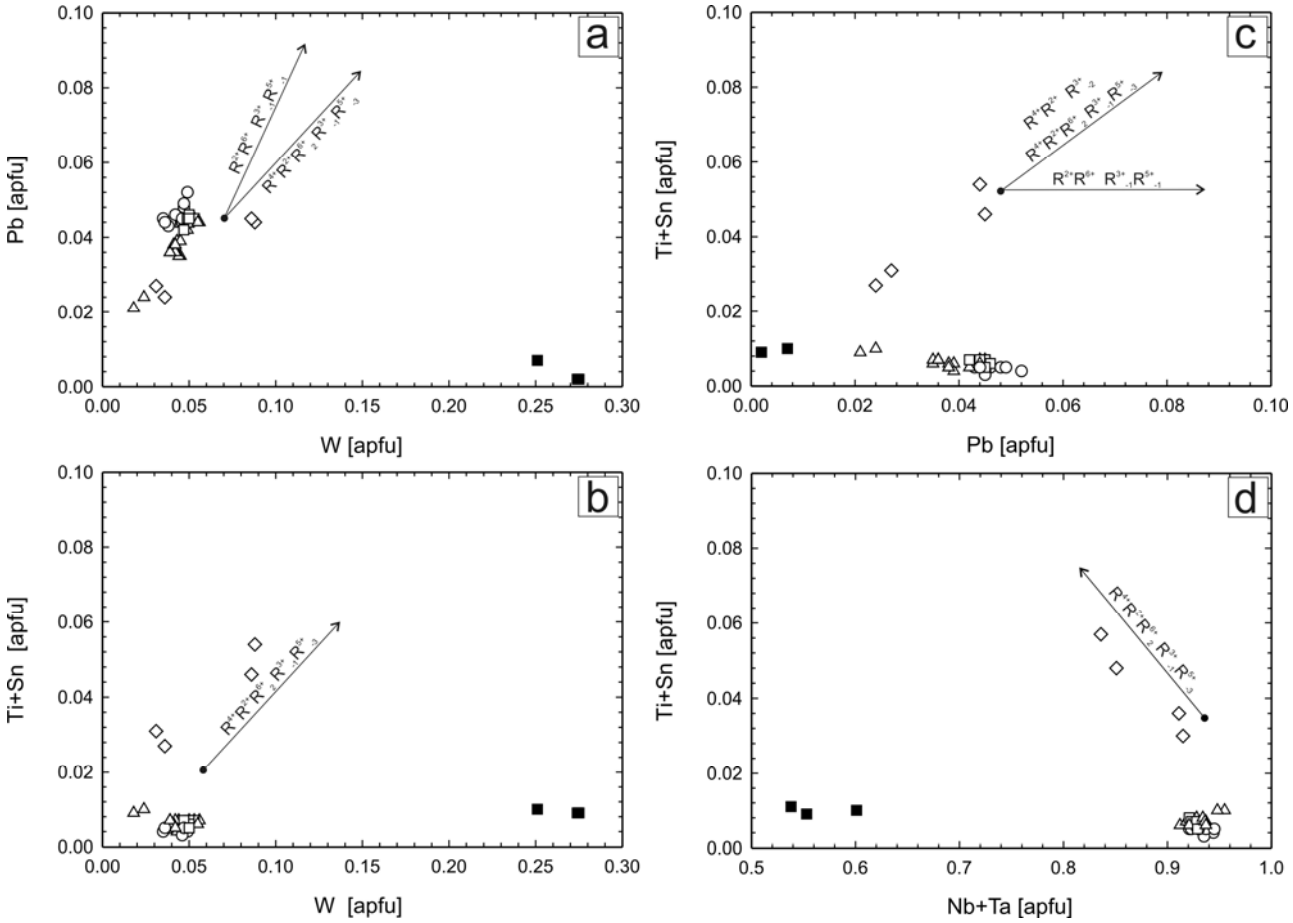

Fig. 4. Plots Pb *versus* W, Ti+Sn *versus* W, Ti+Sn *versus* Pb, and Ti+Sn *versus* Nb+Ta in the individual phases of the bismutotantalite-stibiotantalite-stibiocolumbite assemblage. R^{2+} = Pb, R^{3+} = Bi+Sb, R^{4+} = Ti+Sn, R^{5+} = Nb+Ta, R^{6+} = W; otherwise the same symbols as in Fig. 2.

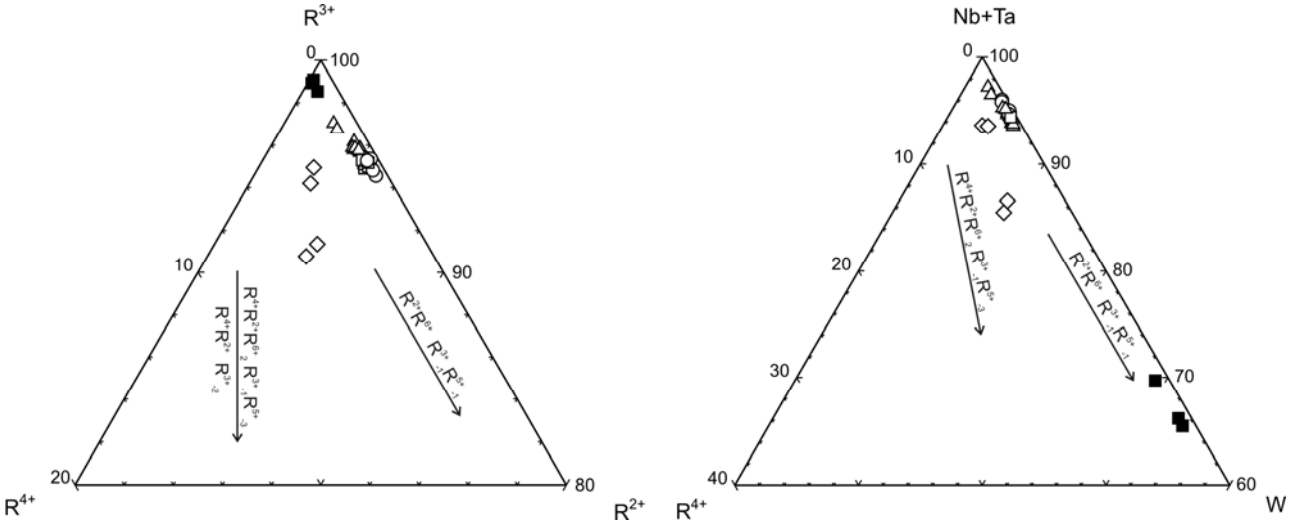

Fig. 5. Compositions of the individual phases of the bismutotantalite-stibiotantalite-stibiocolumbite assemblage in the R^{2+} - R^{3+} - R^{4+} and R^{4+} - R^{5+} - W ternary plots with relevant exchange vectors. R^{2+} = Pb, R^{3+} = Bi+Sb, R^{4+} = Ti+Sn, R^{5+} = Nb+Ta, otherwise the same symbols as in Fig. 2.

Tables:

Table 1. X-ray powder data for primary bismutotantalite-stibiotantalite.

I	d_{obs} (Å)	d_{calc} (Å)	*h*	*k*	*l*	*I*	d_{obs} (Å)	d_{calc} (Å)	*h*	*k*	*l*
1	5.894	5.890	0	2	0	6	2.0297	2.0296	2	4	0
4	4.561	4.563	0	1	1	5	1.9889	1.9888	1	5	1
3	3.709	3.709	1	0	1	2	1.9614	1.9612	1	3	2
27	3.537	3.538	1	1	1	12	1.8949	1.8947	0	4	2
100	3.138	3.139	1	2	1	5	1.8548	1.8546	2	0	2
4	3.076	3.076	0	3	1	10	1.8323	1.8320	2	1	2
58	2.945	2.945	0	4	0	3	1.8029	1.8030	2	5	0
8	2.801	2.801	2	0	0	5	1.7691	1.7690	2	2	2
7	2.724	2.725	2	1	0	8	1.7469	1.7471	3	0	1
8	2.696	2.696	1	3	1	18	1.7353	1.7353	1	6	1
5	2.529	2.529	2	2	0	5	1.7285	1.7282	3	1	1
11	2.475	2.475	0	0	2	1	1.6941	1.6941	2	5	1
1	2.387	2.387	2	1	1	5	1.6768	1.6770	2	3	2
3	2.306	2.306	1	4	1	3	1.6756	1.6749	3	2	1
2	2.280	2.280	2	3	0	1	1.6338	1.6340	0	1	3
1	2.252	2.252	2	2	1	1	1.6325	1.6324	1	5	2
2	2.223	2.223	1	1	2	2	1.6078	1.6077	2	6	0
1	2.127	2.127	0	5	1	3	1.5963	1.5962	3	3	1
1	2.114	2.113	1	2	2	6	1.5693	1.5693	2	4	2
1	2.072	2.071	2	3	1						

a = 5.6017(3), b = 11.7802(3), c = 4.9497(3) Å and V = 326.63(2) $Å^3$.

Table 2. Representative chemical compositions of bismutotantalite-stibiotantalite, stibiotantalite blebs, stibiocolumbite veinlets and stibiocolumbite overgrowths.

	I BT	**I** ST	**II** ST	**II** ST	**IIIa** SC	**IIIa** SC	**IIIb** SC	**IIIb** SC	**IV** SC	**IV** SC
WO_3	2.49	3.25	3.07	2.41	3.20	3.49	17.81	18.88	6.86	2.61
Ta_2O_5	34.37	34.07	36.59	38.82	28.68	26.76	16.25	15.55	10.34	21.34
Nb_2O_5	11.44	11.59	13.52	13.13	20.25	21.38	14.62	11.82	30.98	25.51
TiO_2	0.00	0.00	0.00	0.00	0.00	0.00	0.00	0.00	1.20	0.56
UO_2	0.06	0.00	0.03	0.00	0.00	0.00	0.00	0.18	0.29	0.25
SnO_2	0.18	0.28	0.23	0.21	0.28	0.24	0.45	0.41	0.46	0.25
Sb_2O_3	18.38	19.81	38.96	39.09	40.82	40.85	48.96	50.27	46.82	44.40
Bi_2O_3	30.15	28.36	4.13	2.73	3.57	3.23	1.15	0.83	1.00	1.94
As_2O_3	0.00	0.15	0.63	0.57	0.72	0.45	0.91	0.77	0.70	0.60
PbO	2.21	2.64	2.83	2.83	2.96	3.04	0.50	0.14	3.27	1.72
Sum	99.28	100.15	99.99	99.79	100.48	99.44	100.65	98.85	101.92	99.18
recalculation based on 4 oxygens										
W^{6+}	0.042	0.053	0.046	0.036	0.045	0.050	0.251	0.275	0.088	0.036
Ta^{5+}	0.603	0.588	0.571	0.605	0.426	0.399	0.241	0.238	0.140	0.306
Nb^{5+}	0.334	0.332	0.350	0.340	0.500	0.530	0.360	0.300	0.696	0.609
Ti^{4+}	0.000	0.000	0.000	0.000	0.000	0.000	0.000	0.000	0.045	0.022
U^{4+}	0.001	0.000	0.000	0.000	0.000	0.000	0.000	0.002	0.003	0.003
Sn^{4+}	0.005	0.007	0.005	0.005	0.006	0.005	0.010	0.009	0.009	0.005
Sb^{3+}	0.489	0.518	0.921	0.924	0.920	0.923	1.099	1.165	0.959	0.967
Bi^{3+}	0.501	0.464	0.061	0.040	0.050	0.046	0.016	0.012	0.013	0.026
As^{3+}	0.000	0.006	0.022	0.020	0.024	0.015	0.030	0.026	0.021	0.019
Pb^{2+}	0.038	0.045	0.044	0.044	0.044	0.045	0.007	0.002	0.044	0.024
Σ cat.	2.012	2.013	2.020	2.014	2.016	2.011	2.014	2.030	2.017	2.019
O	4	4	4	4	4	4	4	4	4	4
Ta/(Ta+Nb)	0.644	0.639	0.620	0.640	0.460	0.429	0.401	0.442	0.167	0.334
Bi/(Bi+Sb)	0.506	0.473	0.062	0.041	0.052	0.047	0.014	0.010	0.013	0.026

BT – bismutotantalite, ST – stibiotantalite, SC – stibiocolumbite; otherwise the same symbols as in Fig. 3; Ca, Mn and Fe below their detection limits.